Nonlinear V6 schemes for compressible flow

Bruno Koobus, Stephen F. Wornom, Simone Camarri, Maria-Vittoria Salvetti, Alain Dervieux

INSTITUT NATIONAL DE RECHERCHE EN INFORMATIQUE ET EN AUTOMATIQUE

Nonlinear V6 schemes for compressible flow

B. Koobus, S. Wornom, S. Camarri, M.-V. Salvetti, A. Dervieux

N° ????

30 janvier 2008

Thème NUM

ISSN 0249-6399 ISRN INRIA/RR--????--FR+ENG

Nonlinear V6 schemes for compressible flow

B. Koobus*, S. Wornom†, S. Camarri‡, M.-V. Salvetti§, A. Dervieux¶

Thème NUM — Systèmes numériques
Projet Smash

Rapport de recherche n° ???? — 30 janvier 2008 — 34 pages

Abstract: We describe several numerical schemes for conservation laws well adapted to nonlinear aerodynamics. The schemes are vertex centered, dissipative. They apply with second-order accuracy to unstructured tetrahedrizations and extend to higher order (up to sixth) on a certain type of Cartesian triangulations/tetrahedrizations.

Key-words: Aerodynamics, numerical schemes, hyperbolic models, Euler equations, unstructured meshes

* Dept Mathématiques, Univ. Montpellier II, CC.051, 34095 Montpellier, France, and INRIA
† Lemma, 938, avenue de la republique, 06550 La Roquette, France
‡ Dipl. Ingegneria Aerospaziale, Via Caruso,56126 Pisa (Italy)
§ Dipl. Ingegneria Aerospaziale, Via Caruso,56126 Pisa (Italy)
¶ INRIA, 2004 Route des Lucioles, BP. 93, 06902 Sophia-Antipolis, France

Unité de recherche INRIA Sophia Antipolis
2004, route des Lucioles, BP 93, 06902 Sophia Antipolis Cedex (France)
Téléphone : +33 4 92 38 77 77 — Télécopie : +33 4 92 38 77 65

Schémas V6 non-linéaire pour les écoulement compressibles

Résumé : Ce rapport décrit plusieurs schémas numériques bien adaptés à l'aérodynamique nonlinéaire. Ces schémas sont centrés sommet, dissipatifs, précis au second ordre sur des tetraédrisations non-structurées et d'un ordre plus élevé (jusqu'à six) sur un certain type de triangulation et tétraédrisation cartésiennes.

Mots-clés : Aérodynamique, schémas numériques, modèles hyperboliques, équations d'Euler, maillages non-structurés

1 Introduction

The present work is part of a research program aimed at proposing numerical schemes suitable for the simulation of a class of complex compressible flow models. In this class of complex flow models we include Large Eddy Simulation models and, for the longer term, nonlinear aeroacoustics. We also include complex geometries and various scales, so that unstructured meshes should also be accounted for.
This paper is the sequel of a series of works focusing on the numerical simulation of turbulent flows with second-order schemes which apply on unstructured meshes, and are equipped with a very low dissipative term, see [11],[9],[10]. It also inherits from previous investigations concerning the numerical simulation of the propagation of acoustic waves with first-order partial differential equations of hyperbolic type, see [21].
As for space discretization, we will consider regular meshes in regions where the flow is smooth or homogenous, and unstructured meshes in cases where this option can be more efficient and manageable.
The case of regular meshes is an easier one. In the case of the advection with constant velocity, to find a good advection scheme reduces essentially to finding a good interpolation scheme. In the case of a Courant number equal to 1., some schemes can even be exact. Dispersion effects can be mastered without much numerical dissipation. High-order schemes are easier to build and less computer intensive.
The case of unstructured meshes represents the most difficult one. First, mesh irregularity amplifies dispersion phenomena. Secondly, many useful numerical methods do not extend easily (traditional compact schemes, for example) to the "unstructured" case. The combination of nonlinear first-order hyperbolic problems and unstructured meshes is generally addressed with methods involving dissipation, which are obtained from extensions of Godunov methods. Today, essentially two families of schemes enjoy high-order of accuracy, conservation properties and dissipation ones, viz. the adaptation of ENO-type schemes to unstructured meshes ([6]), and the Discontinuous-Galerkin method ([8]). These high-order methods apply to any unstructuerd mesh at the cost of an important extra complexity. This point is analysed for ENO in [13]. According to this work, these two families of schemes are more accurate than previous methods mainly when they are of fourth-order ([13]). In that case, they are efficient only when enough nodes are used and a very small error is demanded.
From these remarks we can derive the following recommandations for unstructured meshes:
- (i) build second-order schemes that involve small dissipation comparable high-order schemes,
- (ii) equip the second-order scheme of superconvergence properties on Cartesian meshes and use as often as possible Cartesian grids in subregions of the computational domain.
By superconvergence properties we mean that the scheme applies to arbitrary unstructured meshes but in region where the mesh is Cartesian, the truncation error is smaller by several orders of magnitude. As far as (i) is concerned, we emphasize that the task is complex. Indeed, dissipation should offer a compensation to dispersion in the sense that excessively dispersed high frequencies should be damped in order to avoid oscillations and large errors.
In [16], we have introduced 2D versions of a new family of schemes. In [1, 2, 3, 4, 5] a higher order extension to 2D variable coefficients and nonlinear case is built and applied. In [21], a

3D version that is superconvergent for linear advection is introduced. We examine here for the 3D case several nonlinear extensions.

2 Low dissipation advection schemes : 1D

Monotonous upwind schemes of Godunov type enjoy a lot of interesting qualities due to the perfect adequacy of the involved upwinding to unsteady waves. Unfortunately, the amount of dissipation which they introduce seems much larger than that needed to obtain an accurate non-oscillatory numerical solution. As a consequence, the dominant term of the numerical error is carried by the dissipation.

We suggest to forget about strict monotonicity and to get inspired by Direct Simulation techniques in which non-dissipative high-order approximations are stabilised in good accuracy conditions thanks to filters which rely on very-high even order derivatives. We shall first show how this can be done through a one-dimensional high-order MUSCL method, modified in such a manner that the dominant dissipation term is proportional to a sixth-order derivative in space. In the linear case, this is exactly the construction of [16] also used in [17].

2.1 Spatial 1D MUSCL formulation

Let us first consider the one-dimensional scalar conservation law

$$u_t \, + \, f(u)_x \, = \, 0 \tag{1}$$

As in a MUSCL approximation, a mixed finite-difference/finite-volume method is used for the discretization in space. Let x_j , $1 \leq j \leq N$ denote the discretization points of the mesh. For each discretization point, we state : $u_j \approx u(x_j)$ and we define the control volume C_j as the interval $[x_{j-\frac{1}{2}}, x_{j+\frac{1}{2}}]$ where $x_{j+\frac{1}{2}} \, = \, \dfrac{x_j \, + \, x_{j+1}}{2}$.

As in a finite-difference method, we define the unknown vector $U \, = \, \{u_j\}$ as point approximation values of the function $u(x)$ in each node j of the mesh. The time advancing is written:

$$U_{j,t} \, + \, \Psi_j(U) \, = \, 0 \tag{2}$$

where, similarly to finite volumes, the vector $\Psi(U)$ is built according to approximations of $f(u)$ defined at cell boundaries:

$$\Psi_j(U) \, = \, \frac{1}{\Delta x}(\Phi_{j+\frac{1}{2}} - \Phi_{j-\frac{1}{2}}) \; ; \; \Phi_{j+\frac{1}{2}} \, = \, \Phi(u_j, u_{j+1}, f_{j+\frac{1}{2}^-}, f_{j+\frac{1}{2}^+}) \tag{3}$$

where

$$\Phi(u, v, f, g) \, = \, \frac{1}{2}\,[\,(1 + \delta sign(c))f \, + \, (1 - \delta sign(c))g\,] \;\; , \;\; c = f'(u/2 + v/2).$$

Let us write down a particular flux:

$$\Phi_{j+\frac{1}{2}} \;=\; \Phi(u_j, u_{j+1}, f_{j+\frac{1}{2}^-}, f_{j+\frac{1}{2}^+}) \;=\; \frac{f_{j+\frac{1}{2}^-} + f_{j+\frac{1}{2}^+}}{2} \;+\; \delta sign(c)\frac{f_{j+\frac{1}{2}^-} - f_{j+\frac{1}{2}^+}}{2}\;. \quad (4)$$

The coefficient δ controls the spatial dissipation. For defining the integration values $f_{j\pm\frac{1}{2}^\pm}$ of f at boundaries of control volume C_j, we apply the MUSCL methodology ([24]), to the left and right control volume boundary fluxes; $f_{j\pm\frac{1}{2}^\pm}$ is built using linear interpolation formulas :

$$\begin{array}{lll} f_{j+\frac{1}{2}^-} \;=\; f_j \;+\; \frac{1}{2}\,\Delta f_{j+\frac{1}{2}^-} & ; & f_{j+\frac{1}{2}^+} \;=\; f_{j+1} \;-\; \frac{1}{2}\,\Delta f_{j+\frac{1}{2}^+} \\ f_{j-\frac{1}{2}^-} \;=\; f_{j-1} \;+\; \frac{1}{2}\,\Delta f_{j-\frac{1}{2}^-} & ; & f_{j-\frac{1}{2}^+} \;=\; f_j \;-\; \frac{1}{2}\,\Delta f_{j-\frac{1}{2}^+} \end{array}$$

where $\Delta f_{j\pm\frac{1}{2}^\pm}$ are slopes, i.e. approximations of difference term $\dfrac{\partial f}{\partial x}\Delta x$:

$$\begin{array}{rcl} \Delta f_{j+\frac{1}{2}^-} & = & (1-\beta)\,(f_{j+1} - f_j) \;+\; \beta\,(f_j - f_{j-1}) \\ \Delta f_{j+\frac{1}{2}^+} & = & (1-\beta)\,(f_{j+1} - f_j) \;+\; \beta\,(f_{j+2} - f_{j+1}) \end{array} \quad (5)$$

in which β is an upwinding parameter that controls the combination of fully upwind and centered slopes. For $\beta \;=\; 1/3$ the scheme is the standard third-order accurate scheme.

We observe that if the fluxes are based on polynomial reconstruction from the average values of the unknowns, as in ENO finite volumes, choosing a higher-order reconstruction will produce a higher-order finite-volume scheme. In the present vertex-centered context, high-order accuracy is not obtained by a higher-order interpolation but by an interpolation that compensates the error coming from the final central differencing in (3). This writes as follows:

$$\begin{array}{rcl} \Delta f_{j+\frac{1}{2}^-} & = & (1-\beta)\,(f_{j+1} - f_j) \;+\; \beta\,(f_j - f_{j-1}) \\ & & +\,\theta^c\,(-f_{j-1} \;+\; 3f_j \;-\; 3f_{j+1} \;+\; f_{j+2}\,) \\ & & +\,\theta^d\,(-f_{j-2} \;+\; 3f_{j-1} \;-\; 3f_j \;+\; f_{j+1}\,) \\ \Delta f_{j+\frac{1}{2}^+} & = & (1-\beta)\,(f_{j+1} - f_j) \;+\; \beta\,(f_{j+2} - f_{j+1}) \\ & & +\,\theta^c\,(-f_{j-1} \;+\; 3f_j \;-\; 3f_{j+1} \;+\; f_{j+2}\,) \\ & & +\,\theta^d\,(-f_j \;+\; 3f_{j+1} \;-\; 3f_{j+2} \;+\; f_{j+3}\,) \end{array} \quad (6)$$

where θ^c and θ^d are parameters that control the combination of fully upwind and centered corrections. In order to analyse more simply this scheme, we assume that

$$c \;=\; f'(u) \text{ is constant and equal to } 1\;.$$

Schemes	ω	δ	β	θ^c	θ^d	**Order**
1	0	1	1/3	0	0	3
2	0	1	1/3	- 1/6	0	4
3	0	1	1/3	0	- 1/6	4
4	0	1	1/3	- 1/10	- 1/15	5
4'	0	0	1/3	- 1/10	- 1/15	6
5	1	1	0	0	0	4

Table 1: Accuracy of different versions of the new schemes in 1D case; coefficients are defined in Section 2.1. and 2.2.

Then:

$$\begin{aligned}
\Psi_j(U) \;=\; \frac{1}{4\Delta x}\Big(& \quad (1+\delta)\theta^d & f_{j-3} \\
+ & \quad [(1+\delta)\beta + 2\delta\theta^c - 4\delta\theta^d - 4\theta^d] & f_{j-2} \\
+ & \quad [-2(\beta+2\delta\beta+1) - 8\delta\theta^c + 5\theta^d + 7\delta\theta^d] & f_{j-1} \\
+ & \quad [6\delta\beta + 12\delta\theta^c - 8\delta\theta^d] & f_j \\
+ & \quad [2(\beta-2\delta\beta+1) - 8\delta\theta^c - 5\theta^d + 7\delta\theta^d] & f_{j+1} \\
+ & \quad [-(1-\delta)\beta + 2\delta\theta^c - 4\delta\theta^d + 4\theta^d] & f_{j+2} \\
& \quad -(1-\delta)\theta^d & f_{j+3} \\
& & \Big) \qquad (7)
\end{aligned}$$

which gives:

$$\Psi_j(U) \;=\; \frac{\partial f}{\partial x} + C_3\frac{\Delta x^2}{6}\frac{\partial^3 f}{\partial x^3} + C_4\frac{\Delta x^3}{4}\frac{\partial^4 f}{\partial x^4} + C_5\frac{\Delta x^4}{120}\frac{\partial^5 f}{\partial x^5} + C_6\frac{\Delta x^5}{24}\frac{\partial^6 f}{\partial x^6} + O(\Delta x^6)$$

where

$$\begin{aligned}
C_3 &= 1-3\beta \\
C_4 &= \delta(\beta + 2\theta^c + 2\theta^d) \\
C_5 &= 1 - 15\beta - 60\theta^d \\
C_6 &= \delta(\beta + 2\theta^c + 8\theta^d) \quad .
\end{aligned}$$

We observe that schemes described in (3)-(6) are in general second-order accurate but they become high-order accurate for some values of the parameters β, δ, θ^c and θ^d. Fifth-order accuracy is obtained with an adequate choice of the three coefficients, viz. $\beta = 1/3, \theta_c = -1/10, \theta^d = -1/15$. In that case, the numerical dissipation takes the form:

$$D_j(U) \;=\; \frac{\delta}{60\Delta x}(-f_{j-3} + 6f_{j-2} - 15f_{j-1} + 20f_j - 15f_{j+1} + 6f_{j+2} + f_{j+3} \quad) \qquad (8)$$

The corresponding dissipative flux writes:

$$\bar{D}_{j+\frac{1}{2}}(U) \;=\; \frac{\delta}{60}(-f_{j-2}+5f_{j-1}-10f_j+10f_{j+1}-5f_{j+2}+f_{j+3}\;)\;. \tag{9}$$

Since this dissipation term is based on an upwinding paradigm, it has good explicit linear stability (analysed in the sequel), together with a balanced spatial stabilisation property. In the case where the upwinding paradigm is not invoked in the design of a particular scheme, we can try to get inspired by (9).
Putting $\delta = 0$, leads to a central-differenced (non-dissipative) sixth-order accurate scheme.

2.2 Central differencing and dissipation

The usual central-differences three-point scheme is penalized by a dispersion leading error. This error is compensated in the case where we introduce the finite-element P_1 consistent mass matrix with a weight ω to be chosen between 0 and 1. The time advancing is written:

$$M_\omega U(t) \;+\; \Delta x \Psi(U) \;=\; 0 \tag{10}$$

$$(M_\omega U(t))_j \;=\; (1-\omega)U_{j,t}+\omega m_{j,j-1}U_{j-1,t}+\omega m_{j,j}U_{j,t}+\omega m_{j,j+1}U_{j+1,t}$$

where

$$\begin{aligned} m_{j,j-1} &= 1/6\Delta x \\ m_{j,j} &= 2/3\Delta x \\ m_{j,j+1} &= 1/6\Delta x\;. \end{aligned} \tag{11}$$

Then we can combine this time derivative with a flux as defined above, with the coefficients β,θ^c and θ^d chosen equal to zero. A fourth-order accurate central-differenced scheme is obtained with these options ($\omega = 1$, $\beta = 0$, $\theta^c = \theta^d = 0$). However, this scheme lacks dissipation for our purposes, we propose to add a sixth-order derivative. In order to prepare an extension to gas dynamics, we introduce this dissipation into the simplified Riemann solver Φ. This is done with the following two ingredients:
(i)- a unique extrapolation $f_j/2 + f_{j+1}/2$ of the flux for both left state and right state,
(ii)- the same fifth-order derivatives $T_{j+1/2}/2$ for left and right state, but with different signs.
This writes:

$$\begin{aligned} \Phi(u,v,f,g) &= \frac{1}{2}\left[\,(1+\delta sign(c))f \;+\; (1-\delta sign(c))g\,\right] \;\;,\;\; c=f'(u/2+v/2) \\ f &= f^+_{j+1/2} = f_j/2+f_{j+1}/2+T_{j+1/2}/2 \\ g &= f^-_{j+1/2} = f_j/2+f_{j+1}/2-T_{j+1/2}/2\;. \end{aligned} \tag{12}$$

Terms $f_j/2 + f_{j+1}/2$ will contribute to the central differenced flux, while terms $T_{j+1/2}/2$ will appear only in dissipative terms and finally give the sixth-order dissipation. According to the Pascal triangle, a fifth-order difference evaluated between j and $j+1$ can be written as follows ($C > 0$):

$$T_{j+1/2} = C(-f_{j-2} + 5f_{j-1} - 10f_j + 10f_{j+1} - 5f_{j+2} + f_{j+3}) \tag{13}$$

introducing $\bar{\delta} f_{k,k-1} = f_k - f_{k-1}$ we get:

$$T_{j+1/2} = C(\bar{\delta} f_{j-1,j-2} - 4\bar{\delta} f_{j,j-1} + 6\bar{\delta} f_{j+1,j} - 4\bar{\delta} f_{j+2,j+1} + \bar{\delta} f_{j+3,j+2})$$

introducing the central difference $\bar{\delta} f_k = 0.5\bar{\delta}_{k+1,k} + 0.5\bar{\delta} f_{k,k-1}$ we get:

$$T_{j+1/2} = C(2\bar{\delta} f_{j-1} - 5\bar{\delta} f_{j,j-1} + 6\bar{\delta} f_{j+1,j} - 5\bar{\delta} f_{j+2,j+1} + 2\bar{\delta} f_{j+2})$$

In order to introduce the same level of dissipation as in the upwind case (8), we choose the constant C as:

$$C = \frac{c\delta}{60} \ .$$

2.3 Time advancing stability

2.3.1 With a diagonal mass matrix

We can combine the above scheme with the standard Runge-Kutta time advancing.

$$\begin{array}{l} U^{(0)} = U^n \\ V_1 = \Delta t \ \Psi(U^n) \\ V_2 = \Delta t \ \Psi(U^n + V_1/2) \\ V_3 = \Delta t \ \Psi(U^n + V_2/2) \\ V_4 = \Delta t \ \Psi(U^n + V_3) \\ U^{n+1} \ = \ U^n + V_1/6 + V_2/3 + V_3/3 + V_4/6 \end{array} \tag{14}$$

In many case a linearized version can be used. Let us recall the Jameson variant ([23]) which applied to any number of stage and writes as follows:

$$\begin{array}{l} U^{(0)} = U^n \\ U^{(k)} = U^{(0)} + \dfrac{\Delta t}{N-k+1} \Psi\left(U^{(k-1)}\right), \quad k = 1 \ldots N \\ U^{n+1} = U^{(N)} \end{array} \tag{15}$$

We recall in Table 2 some typical maximal CFL numbers for the six-stage RK scheme, which ensure a global accuracy of five for the two best schemes of the proposed family. This table illustrates that the above schemes can be used with CFL number of the order of the unity.

ω	β	θ^c	θ^d	δ	CFL_{max}
0				1	1
0	1/3	0	0	1	2.310
0	1/3	- 1/6	0	1	0.263
0	1/3	0	- 1/6	1	1.332
0	1/3	- 1/10	- 1/15	1	1.867
1	0	0	0	1	.303

Table 2: Maximal Courant numbers (explicit RK6 scheme) for the four different FV-V6 and the FE-V6 spatial schemes(1D analysis)

2.3.2 With a consistent mass matrix

The stable time steps of diagonal mass-matrix version do not apply to the mass-consistent case,

$$\begin{aligned} &U^{(0)} = U^n \\ &U^{(k)} = U^{(0)} + \frac{\Delta t}{N-k+1} M_\omega^{-1} \Psi\left(U^{(k-1)}\right), \quad k = 1 \dots N \\ &U^{n+1} = U^{(N)} \end{aligned} \tag{16}$$

see (Tab.2).

2.3.3 Implicit time stepping

All of these schemes can be advanced in time with implicit schemes such as BDF1 and BDF2, see [15]. Combination with Defect Correction ([20]) is also possible. Linear stability is unconditional in all cases.

3 Unstructured two-dimensional case

The family of 2D schemes that is considered is a *mixed finite-volume finite-element approximation*, applying on triangulations, and of *vertex-centered* type. We refer to [18] for a detailed description of this family of scheme.

3.1 Dual finite volume

Around each vertex is built a cell following to main options:
- either the cell is limited by part of the medians of surrounding triangles,
- or the cell is built according to an idea of Barth ([7]) by joining the center of edges with the center of the smallest circle containing the considered triangle.

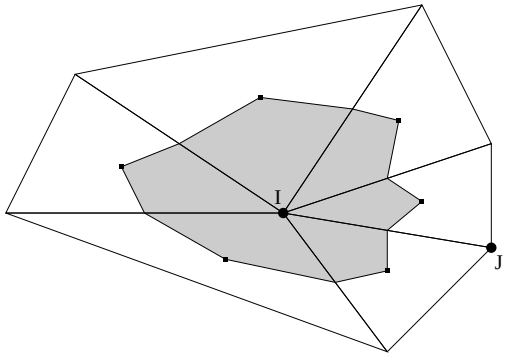

Figure 1: Median cell construction

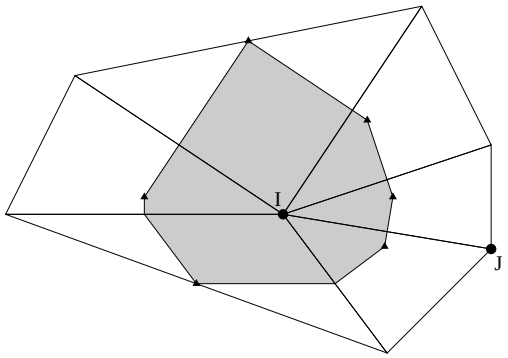

Figure 2: Circumcenter "Barth" cell construction

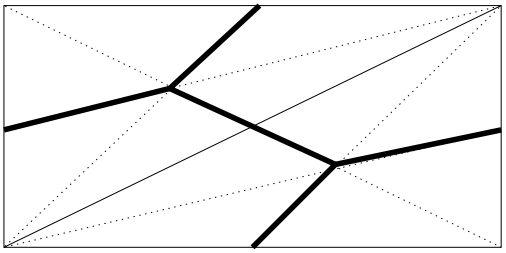

Figure 3: Trace of the medians division on two Friedrichs-Keller elements

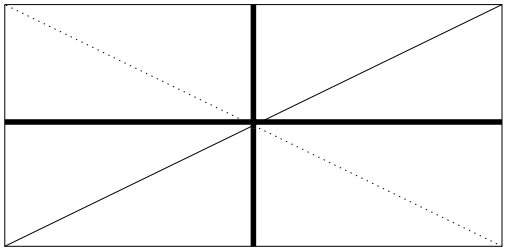

Figure 4: Trace of Barth division on two Friedrichs-Keller elements

The fluxes are assembled on an edge-based process, i.e. for each edge ij between two nodes i and j, and then summed for each node i as follows:

$$meas(C_i)\ W_{i,t} \quad F \quad + \Sigma \quad \Phi_{ij} \quad = \quad 0 \tag{17}$$

where Φ_{ij} are elementary fluxes computed with Riemann solvers.
We first recall the features of an extended version proposed in [16], [17] for Euler calculations.

The numerical integration of a finite-volume upwind scheme with constant-by-cell interpolation generally leads to approximations which are only first-order accurate. The MUSCL methodology of van Leer has been extended to vertex-centered unstructured formulations in order to reach second order accuracy (see for example [18]). This extension relies on the evaluation fluxes with extrapolated values F_{ij}, F_{ji} at the interface of the cells (Figure 5): with:

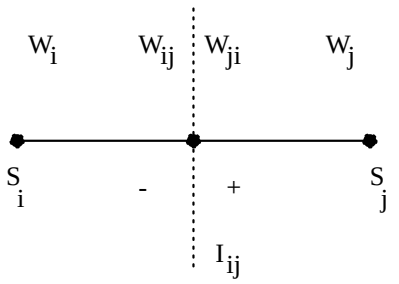

Figure 5: Position of F_{ij} and F_{ji} on [S_i,S_j]

$$\left\{ \begin{array}{rcl} F_{ij} & = & F_i + 0.5\ (\vec{\nabla} F)_{ij}.\vec{ij} \\ F_{ji} & = & F_j - 0.5\ (\vec{\nabla} F)_{ji}.\vec{ij} \end{array} \right. \tag{18}$$

where the "extrapolation slopes" $(\vec{\nabla}\, F)_{ij,ji}$ are obtained using a combination of centered and upwind gradients.

In order to increase the accuracy of the basic MUSCL construction, we propose to define these slopes as follows :
The centered gradient $(\vec{\nabla} F)^c_{ij}$ is defined as $(\vec{\nabla} F)^c_{ij}\,.\,\vec{ij} = F_j - F_i$.
The nodal gradient $(\vec{\nabla} F)_i$ is calculated on the cell C_i as the average of the gradients of the triangles which include the considered node :

$$(\vec{\nabla} F)_i = \frac{1}{meas(C_i)} \sum_{T \in C_i} \frac{meas(T)}{3} \sum_{k \in T} F_k\, \vec{\nabla}\, \Phi^T_k \tag{19}$$

In order to define other approximations of the gradients, let us define the upwind and downwind triangles T_{ij} and T_{ji}. The element T_{ij} is ***upwind*** to the vertex i with respect to the edge ij if, for any sufficiently small positive number η, the vector $-\eta\vec{ij}$ starting from S_i is inside the element T_{ij}. Symmetrically, the element T_{ji} is ***downwind*** to the vertex i with respect to the edge ij if, for any sufficiently small positive number η, the vector $\eta\vec{ji}$ starting from S_j is inside the element T_{ji}. With reference to Figure 6, let ϵ_{ni}, ϵ_{mi}, ϵ_{jr} and ϵ_{js} be the components of vector $\vec{ji}$ (resp. $\vec{ij}$) in the oblique system of axes $(\vec{in}, \vec{im})$ (resp. $\vec{jr}, \vec{js}$)):

$$\vec{ji} = \epsilon_{ni}\, \vec{in} + \epsilon_{mi}\, \vec{im}\,,$$

$$\vec{ij} = \epsilon_{jr}\, \vec{jr} + \epsilon_{js}\, \vec{js}\,.$$

Then saying that T_{ij} and T_{ji} are upstream and downstream elements means that they have been chosen in such a way that the components ϵ_{ri}, etc. are all nonnegative:

$$T_{ij} \text{ upwind and } T_{ji} \text{ downwind} \Leftrightarrow \epsilon_{ni}, \epsilon_{mi}, \epsilon_{jr}, \epsilon_{js} \text{ are all non-negative.}$$

The upwind gradient $(\vec{\nabla}F)^u_{ij}$ is computed as the usual finite-element gradient on T_{ij} and the downwind gradient $(\vec{\nabla}F)^d_{ij}$ on T_{ji}. This writes :
$(\vec{\nabla}F)^u_{ij} = \vec{\nabla}F\,|_{T_{ij}}$ and $(\vec{\nabla}F)^d_{ij} = \vec{\nabla}F\,|_{T_{ji}}$ where $\vec{\nabla}F\,|_T = \sum_{k\in T} F_k \vec{\nabla}\Phi_k|_T$ are the P1-Galerkin gradients on triangle T. This option allows extensions to Local Extremum Diminishing (LED) schemes as shown in [23] [14].
We also need to define:

$$(\vec{\nabla}F)^c_{ij}.\vec{ij} = F_j - F_i \ .$$

We now specify our method for computing the extrapolation slopes $(\vec{\nabla}F)_{ij}$ and $(\vec{\nabla}F)_{ji}$:

$$\begin{aligned}(\vec{\nabla}F)_{ij}.\vec{ij} = \quad & (1-\beta)(\vec{\nabla}F)^c_{ij}.\vec{ij} + \beta(\vec{\nabla}F)^u_{ij}.\vec{ij} \\ & +\xi_c\left[(\vec{\nabla}F)^u_{ij}.\vec{ij} - 2(\vec{\nabla}F)^c_{ij}.\vec{ij} + (\vec{\nabla}F)^d_{ij}.\vec{ij}\right] \\ & +\xi_d\left[(\vec{\nabla}F)_{D^*_{ij}}.\vec{ij} - 2(\vec{\nabla}F)_i.\vec{ij} + (\vec{\nabla}F)_j.\vec{ij}\right] \ ,\end{aligned} \tag{20}$$

The computation of F_{ji} is analogous:

$$\begin{aligned}(\vec{\nabla}F)_{ji}.\vec{ij} = \quad & (1-\beta)(\vec{\nabla}F)^c_{ij}.\vec{ij} + \beta(\vec{\nabla}F)^d_{ij}.\vec{ij} \\ & +\xi_c\left[(\vec{\nabla}F)^u_{ij}.\vec{ij} - 2(\vec{\nabla}F)^c_{ij}.\vec{ij} + (\vec{\nabla}F)^d_{ij}.\vec{ij}\right] \\ & +\xi_d\left[(\vec{\nabla}F)_{D^*_{ji}}.\vec{ij} - 2(\vec{\nabla}F)_j.\vec{ij} + (\vec{\nabla}F)_i.\vec{ij}\right] \ ,\end{aligned} \tag{21}$$

The term $\left(\vec{\nabla}F\right)_{D^*_{ij}}$ is the gradient at the point D^*_{ij}. This last gradient is computed by interpolation of the nodal gradient values at the nodes contained in the face opposite to i in the upwind triangle T_{ij}.

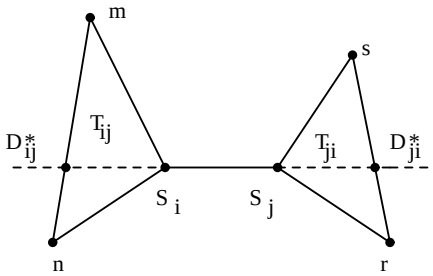

Figure 6: Localisation of the extra interpolation points D^*_{ij} and D^*_{ji} of nodal gradients

The coefficients β, ξ^c and ξ^d are upwinding parameters that control the combination of fully upwind and centered slopes.

3.2 Consistent-mass variant

A important variant of the above scheme involves a time derivative that is evaluated with the finite-element consistent mass matrix, expressed in terms of the usual P_1 test functions as follows:

$$M_{ij}^{FEM} = \int \psi_i \psi_j \, dv \tag{22}$$

which carries an extra parameter ω equal to 1 when the matrix is from FEM, 0 when we keep the previous diagonal one:

$$\begin{aligned} M_{ij}^{\omega} &= \omega \int \psi_i \psi_j \, dv + (1-\omega) M_i^{FVM} j \\ M_i^{FVM} j &= meas(C_i) \quad if \quad i = j, \quad 0 \quad else. \end{aligned}$$

3.3 Analysis of Cartesian case (2D/median/2D/Barth)

We have introduced a discretization of the spatial flux, which is parameterized with the coefficients β, ξ^c, ξ^d and δ. We have also introduced a discretization of the time derivative, parameterized with a coefficient ω as a weight between a diagonal finite-volume-like mass matrix and a finite-element one. We restrict to an advection model:

$$U_t + aU_x + bU_y = 0 \ . \tag{23}$$

We denote by $U^{\beta,\delta,\omega,\xi_c,\xi_d}$ the discrete solution of (23) obtained by applying the above scheme with the parameters $(\beta, \delta, \omega, \xi_c, \xi_d)$. Let us give a few truncation error calculations.

3.3.1 Basic beta-delta-scheme

$$\begin{aligned} U_t^{\beta,\delta,0,0,0} = & -aU_x - bU_y \\ & +T_2 \\ & +T_3 \\ & +T_4 \\ & +T_5 \\ & +O(\Delta x^6, \frac{\Delta x^7}{\Delta y}, \frac{\Delta y^7}{\Delta x}, \Delta y^6) \end{aligned} \tag{24}$$

with the following second-order term:

$$\begin{aligned} T_2 \quad = \quad & \\ & +\frac{a}{6}(3\beta-1)\Delta x^2 \quad U_{xxx} \\ & +\frac{(3\beta-1)}{6}C_1\Delta x \quad U_{xxy} \\ & +\frac{(3\beta-1)}{6}C_1\Delta y \quad U_{xyy} \\ & +\frac{b}{6}(3\beta-1)\Delta y^2 \quad U_{yyy} \end{aligned}$$

with the following third-order term:

$$\begin{aligned} T_3 \quad = \quad & \\ & -\delta\left(\frac{\beta}{12}\right)C_2\frac{\Delta x^3}{\Delta y} \quad U_{xxxx} \\ & -\delta\left(\frac{\beta}{3}\right)|C_1|\Delta x^2 \quad U_{xxxy} \\ & -\delta\left(\frac{\beta}{3}\right)|C_1|\Delta x\Delta y \quad U_{xxyy} \\ & -\delta\left(\frac{\beta}{3}\right)|C_1|\Delta y^2 \quad U_{xyyy} \\ & -\delta\left(\frac{\beta}{12}\right)C_3\frac{\Delta y^3}{\Delta x} \quad U_{yyyy} \end{aligned}$$

with the following fourth-order term:

$$\begin{aligned} T_4 \quad = \quad & \\ & a\frac{\beta}{8}\Delta x^4 \quad U_{xxxxx} \\ & \left(\frac{5\beta}{24}-\frac{1}{72}\right)C_1\Delta x^3 \quad U_{xxxxy} \\ & \left(\frac{5\beta}{12}-\frac{1}{36}\right)C_1\Delta x^2\Delta y \quad U_{xxxyy} \\ & \left(\frac{5\beta}{12}-\frac{1}{36}\right)C_1\Delta x\Delta y^2 \quad U_{xxyyy} \\ & \left(\frac{5\beta}{24}-\frac{1}{72}\right)C_1\Delta y^3 \quad U_{xyyyy} \\ & b\frac{\beta}{8}\Delta y^4 \quad U_{yyyyy} \end{aligned}$$

and the following fifth-order term:

$$\begin{aligned} T_5 \quad = \quad & \\ & -\delta\frac{\beta}{72}C_2\frac{\Delta x^5}{\Delta y} \quad U_{xxxxxx} \\ & -\delta\frac{\beta}{12}|C_1|\Delta x^4 \quad U_{xxxxxy} \\ & -\delta\frac{5\beta}{24}|C_1|\Delta x^3\Delta y \quad U_{xxxxyy} \\ & -\delta\frac{5\beta}{18}|C_1|\Delta x^2\Delta y^2 \quad U_{xxxyyy} \\ & -\delta\frac{5\beta}{24}|C_1|\Delta x\Delta y^3 \quad U_{xxyyyy} \\ & -\delta\frac{\beta}{12}|C_1|\Delta y^4 \quad U_{xyyyyy} \\ & -\delta\frac{\beta}{72}C_3\frac{\Delta y^5}{\Delta x} \quad U_{yyyyyy} \end{aligned} \tag{25}$$

and where the C_i's are affine in Δx and Δy:

$$\begin{aligned} C_1 &= b\Delta x + a\Delta y \\ C_2 &= |b\Delta x + a\Delta y| + |-b\Delta x + 2a\Delta y| \\ C_3 &= |b\Delta x + a\Delta y| + |+2b\Delta x - a\Delta y| \ . \end{aligned} \tag{26}$$

3.3.2 Analysis of consistent-mass variant

The basic $\beta-\delta-\omega$ scheme involves a diagonal mass-matrix version when $\omega = 0$ and a full consistent mass-matrix for $\omega = 1$. We give now the extra terms introduced by the general case ($\omega \neq 0$):

$$\begin{aligned} U_t^{\beta,\delta,\omega,0,0} - U_t^{\beta,\delta,0,0,0} \quad = \quad & \\ & +P_2 \\ & +P_3 \\ & +P_4 \\ & +P_5 \\ & +O(\Delta x^6, \frac{\Delta x^7}{\Delta y}, \frac{\Delta y^7}{\Delta x}, \Delta y^6) \end{aligned} \tag{27}$$

with the following second-order term:

$$\begin{aligned} P_2 \quad = \quad & \\ & +\frac{a}{6}\omega\Delta x^2 \quad U_{xxx} \\ & +\frac{\omega}{6}C_1\Delta x \quad U_{xxy} \\ & +\frac{\omega}{6}C_1\Delta y \quad U_{xyy} \\ & +\frac{b}{6}\omega\Delta y^2 \quad U_{yyy} \end{aligned}$$

with the following third-order term:

$$P_3 \quad = \quad 0$$

with the following fourth-order term:

$$\begin{aligned} P_4 \quad = \quad & \\ & -a\frac{\omega}{12}(\beta+\frac{\omega}{3}-\frac{1}{2})\Delta x^4 \quad U_{xxxxx} \\ & -\frac{\omega}{6}(\beta+\frac{\omega}{3}-\frac{1}{2})C_1\Delta x^3 \quad U_{xxxxy} \\ & -\frac{\omega}{6}(\beta+\frac{\omega}{3}-\frac{1}{2})C_1\Delta x^2\Delta y \quad U_{xxxyy} \\ & -\frac{\omega}{6}(\beta+\frac{\omega}{3}-\frac{1}{2})C_1\Delta x\Delta y^2 \quad U_{xxyyy} \\ & -\frac{\omega}{6}(\beta+\frac{\omega}{3}-\frac{1}{2})C_1\Delta y^3 \quad U_{xyyyy} \\ & -b\frac{\omega}{12}(\beta+\frac{\omega}{3}-\frac{1}{2})\Delta y^4 \quad U_{yyyyy} \end{aligned}$$

we do not give the further terms and refer to [15]. The above terms allow to verify that for $\beta = 0$ and $\omega = 1$, P_2 and T_2 compensate, P_3 and T_3 vanish, the scheme is fourth accurate.

The scheme is not dissipative and this can carry some stability problems for compressible flows and non-regular meshes. We can add a dissipation term as in Sec. 2.2. An adaptation will rely on dissipation fluxes:

$$T_{ij} = C(2(\vec{\nabla}F)_{D^*_{ij}}.\vec{ij} - 5(\vec{\nabla}F)^u_{ij}.\vec{ij} + 6(\vec{\nabla}F)^c_{ij}.\vec{ij} - 5(\vec{\nabla}F)^d_{ij}.\vec{ij} + 2(\vec{\nabla}F)_{D^*_{ji}}.\vec{ij}) \ .$$

3.3.3 Analysis of ξ_c terms

We assume $\omega = 0$.

$$\begin{aligned} U_t^{\beta,\delta,0,\xi_c,0} - U_t^{\beta,\delta,0,0,0} &= \\ &+Q_2 \\ &+Q_3 \\ &+Q_4 \\ &+Q_5 \\ &+O(\Delta x^6, \frac{\Delta x^7}{\Delta y}, \frac{\Delta y^7}{\Delta x}, \Delta y^6) \end{aligned} \tag{28}$$

with the following second-order term:

$$Q_2 = 0$$

with the following third-order term:

$$\begin{aligned} Q_3 = & \\ & -\delta \left(\frac{\xi_c}{6}\right) C_2 \frac{\Delta x^3}{\Delta y} \quad U_{xxxx} \\ & -\delta \left(\frac{2\xi_c}{3}\right) |C_1| \Delta x^2 \quad U_{xxxy} \\ & -\delta \left(\xi_c\right) |C_1| \Delta x \Delta y \quad U_{xxyy} \\ & -\delta \left(\frac{2\xi_c}{3}\right) |C_1| \Delta y^2 \quad U_{xyyy} \\ & -\delta \left(\frac{\xi_c}{6}\right) C_3 \frac{\Delta y^3}{\Delta x} \quad U_{yyyy} \end{aligned}$$

with the following fourth-order term:

$$Q_4 = 0$$

and the following fifth-order term:

$$
\begin{aligned}
Q_5 \quad = \quad & \\
& -\delta\frac{\xi_c}{36}C_2\frac{\Delta x^5}{\Delta y} \quad U_{xxxxxx} \\
& -\delta\frac{\xi_c}{6}|C_1|\Delta x^4 \quad U_{xxxxxy} \\
& -\delta\frac{5\xi_c}{12}|C_1|\Delta x^3\Delta y \quad U_{xxxxyy} \\
& -\delta\frac{5\xi_c}{9}|C_1|\Delta x^2\Delta y^2 \quad U_{xxxyyy} \\
& -\delta\frac{5\xi_c}{12}|C_1|\Delta x\Delta y^3 \quad U_{xxyyyy} \\
& -\delta\frac{\xi_c}{6}|C_1|\Delta y^4 \quad U_{xyyyyy} \\
& -\delta\frac{\xi_c}{36}C_3\frac{\Delta y^5}{\Delta x} \quad U_{yyyyyy} \ . \qquad (29)
\end{aligned}
$$

3.3.4 Analysis of ξ_d terms

We assume $\omega = 0$.

$$
\begin{aligned}
U_t^{\beta,\delta,0,0,\xi_d} - U_t^{\beta,\delta,0,0,0} \quad = \quad & \\
& +R_2 \\
& +R_3 \\
& +R_4 \\
& +R_5 \\
& +O(\Delta x^6, \frac{\Delta x^7}{\Delta y}, \frac{\Delta y^7}{\Delta x}, \Delta y^6) \qquad (30)
\end{aligned}
$$

with the following second-order term:

$$R_2 \quad = \quad 0$$

with the following third-order term:

$$\begin{aligned} R_3 \quad = \quad & \\ & -\delta \left(\frac{\xi_d}{6}\right) C_2 \frac{\Delta x^3}{\Delta y} \quad U_{xxxx} \\ & -\delta \left(\frac{2\xi_d}{3}\right) |C_1| \Delta x^2 \quad U_{xxxy} \\ & -\delta \left(\xi_d\right) |C_1| \Delta x \Delta y \quad U_{xxyy} \\ & -\delta \left(\frac{2\xi_d}{3}\right) |C_1| \Delta y^2 \quad U_{xyyy} \\ & -\delta \left(\frac{\xi_d}{6}\right) C_3 \frac{\Delta y^3}{\Delta x} \quad U_{yyyy} \end{aligned}$$

with the following fourth-order term:

$$\begin{aligned} R_4 \quad = \quad & \\ & a \frac{\xi_d}{4} \Delta x^4 \quad U_{xxxxx} \\ & \left(\frac{5\xi_d}{12}\right) C_1 \Delta x^3 \quad U_{xxxxy} \\ & \left(\frac{5\xi_d}{6} - \frac{1}{36}\right) C_1 \Delta x^2 \Delta y \quad U_{xxxyy} \\ & \left(\frac{5\xi_d}{6} - \frac{1}{36}\right) C_1 \Delta x \Delta y^2 \quad U_{xxyyy} \\ & \left(\frac{5\xi_d}{12} - \frac{1}{72}\right) C_1 \Delta y^3 \quad U_{xyyyy} \\ & b \frac{\xi_d}{4} \Delta y^4 \quad U_{yyyyy} \end{aligned}$$

and the following fifth-order term:

$$\begin{aligned} R_5 \;=\; & \\ & -\delta\frac{5\xi_d}{72}C_2\frac{\Delta x^5}{\Delta y} \quad U_{xxxxxx} \\ & -\delta\frac{7\xi_d}{18}|C_1|\Delta x^4 \quad U_{xxxxxy} \\ & -\delta\frac{67\xi_d}{72}|C_1|\Delta x^3\Delta y \quad U_{xxxxyy} \\ & -\delta\frac{11\xi_d}{9}|C_1|\Delta x^2\Delta y^2 \quad U_{xxxyyy} \\ & -\delta\frac{67\xi_d}{72}|C_1|\Delta x\Delta y^3 \quad U_{xxyyyy} \\ & -\delta\frac{7\xi_d}{18}|C_1|\Delta y^4 \quad U_{xyyyyy} \\ & -\delta\frac{5\xi_d}{72}C_3\frac{\Delta y^5}{\Delta x} \quad U_{yyyyyy}\ . \end{aligned} \tag{31}$$

We observe in the first term that Δy appears as denominator. Coefficient C_2, see (26), contains a term in Δx. Then the scheme is fifth-order accurate only if the ratio $\Delta x/\Delta y$ is bounded. Conversely, assuming that Δx Δy tends to zero while $(\Delta x)^6/\Delta y$ increases indefinitely, we deduce that the scheme is not consistent for unbounded stretching. From this standpoint, it inherits the consistency problem for stretched meshes which was already noticed in [27].
If we restrict to the case where the second component b of the advection velocity is zero, then $C_2 = 3|a|\Delta y$ and the first term writes:

$$-\delta\frac{5\xi_d}{72}C_2\frac{\Delta x^5}{\Delta y} \quad U_{xxxxxx} = -\frac{15\delta}{72}\xi_d|a|\Delta x^5 \quad U_{xxxxxx}\ . \tag{32}$$

This defines a level of the dissipation coefficient that can be used with stability and accuracy.

3.3.5 Conclusion of analysis

To sum up, the diagonal-mass-matrix schemes, i.e. $\omega = 0$, have only sixth-order dissipation and are in general second-order accurate but they become higher-order accurate for some values of the parameters β (see [19]), ξ^c and ξ^d, see [12] and Table 3. The case of unstructured meshes show the usual behavior for schemes with diagonalised matrix, first-order in general, second-order for smooth variation of mesh size. Better convergence can be observed in practice, we refer to [1]. Also, the level of dissipation of this family of schemes is much smaller than for usual MUSCL schemes, see [16].

The consistent-mass-matrix , i.e. $\omega = 1$ schemes can be made fourth-order accurate. But they are without any dissipation. In order to increase the robustness, particularly for

	ω	β	ξ^c	ξ^d	δ	Order
β-scheme	0	1/3	0	0	1	3
β-scheme	0	1/3	0	0	0	4
FV-V6 Method	0	1/3	-1/30	-2/15	1	5
FE-V6 Method	1	1/3	0	0	1	6

Table 3: Accuracy of different versions of the new scheme in 2D Cartesian case

non-regular meshes, we propose to add a dissipation term based on a sixth-order derivative, and introducting only an extra fifth-order truncation error. In case of unstructured meshes, the finite-element analysis applies and second-order is obtained.

4 Extension to Euler

The Euler equations are denoted by:

$$W_t + div\mathcal{F} = 0 \quad , \quad \mathcal{F} = (F, G) \tag{33}$$

In practice, we need to introduce some dissipation with a Riemann solver. The interest of a good upwinding is a rather rational way in introducing dissipation. The flux difference splitting proposed by Roe writes:

$$(F(U_L) + F(U_R))/2 \; - \; |A(\tilde{U})|(U_R - U_L)/2 \quad , \quad A \; = \; \frac{\partial F}{\partial W}.\vec{n} \; . \tag{34}$$

in which for a diagonalisable matrix $A = T^{-1}\Lambda T$, $|A|$ denotes $T^{-1}|\Lambda|T$ and where $\tilde{U}$ holds for the Roe average of U_R and U_L, in short:

$$\tilde{U} \; = \; (\rho_R^{\frac{1}{2}} U_R + \rho_L^{\frac{1}{2}} U_L / (\rho_R^{\frac{1}{2}} \rho_L^{\frac{1}{2}})$$

which enjoys the following property:

$$F(U_R) - F(U_L) \; - \; A(\tilde{U})(U_R - U_L) \; .$$

In (high enough) supersonic case, $A(\tilde{U}) = |A(\tilde{U})|$ or$A(\tilde{U}) = -|A(\tilde{U})|$ and Roe's splitting is fully upwind. We also observe that

$$|A(\tilde{U})|(U_R - U_L)/2 \; = \; T^{-1} Diag(|\lambda_1|, |\lambda_2|, |\lambda_3|, |\lambda_4|) T \; = \; sign(A) A \; ,$$

where

$$sign(A) \;=\; T^{-1} Diag(sign(\lambda_1), sign(\lambda_2), sign(\lambda_3)) T. \tag{35}$$

thus this averaging also permits the following equivalent formulation:

$$(F(U_L) + F(U_R))/2 \;-\; sign(A(\tilde{U}))(F(U_R) - F(U_L))/2\ . \tag{36}$$

4.1 High-order FV-NLV6 spatial scheme

The algorithm for assembling scheme **FV-NLV6** can be summed up as follows.

0. A background flow $U \;=\; (\rho, \rho u, \rho v, E)$ on each vertex of the mesh are given.

1. Compute the fluxes $\bar{F} \;=\; F(U),\ \bar{G} \;=\; G(U)$ on each vertex (vertexwise loop).

2. Compute the nodal gradients $\nabla\bar{F},\ \nabla\bar{G}$ of the fluxes on each vertex (elementwise loop). This is done by applying the nodal gradient formula:

$$(\vec{\nabla}\bar{F})_i \;=\; \frac{1}{meas(C_i)} \sum_{T \in C_i} \frac{meas(T)}{3} \sum_{k \in T} (\bar{F})_k \,\vec{\nabla}\,\Phi_k^T \tag{37}$$

3. Start *edgewise assembly loop*:
compute the extrapolated slopes :

$$\begin{aligned}(\vec{\nabla}\bar{F})_{ij} \cdot \vec{ij} = \quad & (1-\beta)(\vec{\nabla}\bar{F}))^c_{ij} \cdot \vec{ij} + \beta(\vec{\nabla}\bar{F}))^u_{ij} \cdot \vec{ij} \\ & +\xi_c \left[(\vec{\nabla}\bar{F}))^u_{ij} \cdot \vec{ij} - 2(\vec{\nabla}\bar{F}))^c_{ij} \cdot \vec{ij} + (\vec{\nabla}\bar{F}))^d_{ij} \cdot \vec{ij}\right] \\ & +\xi_d \left[(\vec{\nabla}\bar{F}))_{D^*_{ij}} \cdot \vec{ij} - 2(\vec{\nabla}\bar{F}))_i \cdot \vec{ij} + (\vec{\nabla}\bar{F}))_j \cdot \vec{ij}\right] \quad ,\end{aligned} \tag{38}$$

and analog for $(\vec{\nabla}\bar{F})_{ji}$.
Define flux interpolations:

$$\begin{aligned}\bar{\mathcal{F}} \;&=\; (\bar{F}, \bar{G}) \\ \bar{\mathcal{F}}_{ij} \;&=\; \bar{\mathcal{F}}_i + \frac{1}{2}\nabla\bar{\mathcal{F}}_{ij} \\ \bar{\mathcal{F}}_{ji} \;&=\; \bar{\mathcal{F}}_j - \frac{1}{2}\nabla\bar{\mathcal{F}}_{ji}\end{aligned} \tag{39}$$

The central differenced flux then writes:

$$\Phi_{ij} \;\;=\;\; 0.5\ (\bar{\mathcal{F}}_{ij} \;\;+\;\; \bar{\mathcal{F}}_{ji}) \;\cdot\; n_{ij} \tag{40}$$

4. Evaluate the stabilisation term:

$$\mathcal{D}_{ij} \;=\; 0.5\ \delta\ sign(\mathcal{A}_{ij})(\bar{\mathcal{F}}_{ji} \;\cdot\; n_{ij} - \bar{\mathcal{F}}_{ij} \;\cdot\; n_{ij}) \tag{41}$$

where $\mathcal{A}_{ij}$ is defined by:

$$\mathcal{A}_{ij} \;=\; (F', G')((U_i + U_j)/2) \;\cdot\; n_{ij}. \tag{42}$$

5. Compute the final edge flux as:

$$\Phi_{ij}^{upwind} \;=\; \Phi_{ij} \;-\; \mathcal{D}_{ij} \tag{43}$$

and add (substract) it to flux assembly at vertex i (j).

Remarks:

- We note in passing that choosing flux interpolation allows to escape to the second-order limitation advocated by Wu and Wang ([28]) for MUSCL schemes.
- Positivity holds for the first-order diagonal-mass-matrix version which is the usual upwind scheme. However, a rigourously monotone limited high-order version remains to be found. Consistent-mass-matrix versions are generally not positive.
- As remarked in the analysis (see statement 31), the combination of median cells and upwinding produces inconsistent error terms under the form of quotients $\frac{\Delta x}{\Delta y}$ or $\frac{\Delta y}{\Delta x}$ which can produce large errors when the previous quotient are large, that is when mesh is stretched. One way to escape this inconsistency without losing the low dispersion properties (typically, fifth-order accuracy) consists of using the Barth construction of cells (Section 3.1).

4.2 High-order FE-NLV6 spatial scheme

The algorithm for assembling scheme **FE-NLV6** can be summed up as follows.

0. A background flow $U \;=\; (\rho, \rho u, \rho v, E)$ on each vertex of the mesh are given.

1. Compute the fluxes $\bar{\mathcal{F}} = (\bar{F}, \bar{G}) = (F(U), G(U))$ on each vertex (vertexwise loop).

2. Compute the nodal gradients $\nabla\bar{F},\ \nabla\bar{G}$ of the fluxes on each vertex (elementwise loop). This is done by applying the nodal gradient formula:

$$\begin{aligned}
(\vec{\nabla}\bar{F})_i \;&=\; \frac{1}{meas(C_i)} \sum_{T\,\in\, C_i} \frac{meas(T)}{3} \sum_{k\,\in\, T} (\bar{F})_k\, \vec{\nabla}\, \Phi_k^T \\
(\vec{\nabla}\bar{G})_i \;&=\; \frac{1}{meas(C_i)} \sum_{T\,\in\, C_i} \frac{meas(T)}{3} \sum_{k\,\in\, T} (\bar{G})_k\, \vec{\nabla}\, \Phi_k^T
\end{aligned} \tag{44}$$

3. Start *edgewise assembly loop*: compute the dissipation fluxes:

$$\bar{T}_{ij} = C\left(2(\vec{\nabla}\bar{\mathcal{F}})_{D_{ij}^*} \cdot \vec{ij} - 5(\vec{\nabla}\bar{\mathcal{F}})_{ij}^u \cdot \vec{ij} + 6(\vec{\nabla}\bar{\mathcal{F}})_{ij}^c \cdot \vec{ij} - 5(\vec{\nabla}\bar{\mathcal{F}})_{ij}^d \cdot \vec{ij} + 2(\vec{\nabla}\bar{\mathcal{F}})_{D_{ji}^*}\right) .$$

In order to tune the dissipation to a value close to the one appearing in the upwind scheme (30), with $\xi_c = -1/30,\ \xi_d = -2/15$, we choose:

$$C = \frac{3\delta}{30} \ . \tag{45}$$

Define flux interpolations:

$$\begin{aligned} \bar{\mathcal{F}}_{ij} &= \frac{1}{2}(\bar{\mathcal{F}}_i + \bar{\mathcal{F}}_j) \cdot \ n_{ij} + \bar{T}_{ij} \cdot \ n_{ij} \\ \bar{\mathcal{F}}_{ji} &= \frac{1}{2}(\bar{\mathcal{F}}_i + \bar{\mathcal{F}}_j) \cdot \ n_{ij} - \bar{T}_{ij} \cdot \ n_{ij} \end{aligned} \tag{46}$$

The central differenced flux then writes:

$$\Phi_{ij} \ = \ 0.5 \ (\bar{\mathcal{F}}_{ij} \ + \ \bar{\mathcal{F}}_{ji}) \ \cdot \ n_{ij} \tag{47}$$

4. Evaluate the stabilisation term:

$$\mathcal{D}_{ij} \ = \ 0.5 \ \delta \ ||\bar{n}_{ij}|| \ sign(\mathcal{A}_{ij}) \bar{T}_{ij} \ \cdot \ \bar{n}_{ij} \tag{48}$$

where $\mathcal{A}_{ij}$ is defined by:

$$\mathcal{A}_{ij} \ = \ (F', G')((U_i + U_j)/2) \ \cdot \ \bar{n}_{ij} \tag{49}$$

and where $\bar{n}_{ij}$ is defined later.

5. Compute the final edge flux as:

$$\Phi_{ij}^{upwind} \ = \ \Phi_{ij} \ - \ \mathcal{D}_{ij} \ , \tag{50}$$

add (substract) it to flux assembly at vertex i (j), and multiply by the inverse mass matrix in order to obtain the update of the variable.

- In the same way as in the FV analysis (see statement 31), the use of the normal vector computed from median cells for the dissipation terms will produce inconsistent error terms under the form of quotients $\frac{\Delta x}{\Delta y}$ or $\frac{\Delta y}{\Delta x}$. Passing to Barth cells is not a good idea since we would lose the accuracy benefit of the consistent mass matrix. Our proposal is:
- to keep the FE normal in consistent central fluxes,
- to use as $\bar{n}_{ij}$ the projection of it on edge $\vec{ij}$:

$$\bar{n}_{ij} = \vec{n_{ij}} \cdot \vec{ij} \ \vec{ij} \ .$$

4.3 High-order FE-LV6 spatial scheme

The transformation from linear **LV6** schemes introduced in [15, 16] where the primitive variables are interpolated, into the non-linear **NLV6** schemes introduced in this paper demands an important transformation from a MUSCL scheme, and results in a more computer intensive algorithm. For the case where the used is interested only by a combination of FEM-type approximation with a sophisticated dissipation, we describe now how to assemble a simplified scheme **FE-LV6** with primitive variables interpolation. This writes as follows:

0. A background flow $U = (\rho, \rho u, \rho v, E)$ on each vertex of the mesh is given.

1. Compute the primitive variable $\tilde{U} = (\rho, u, v, p)$ on each vertex (vertexwise loop).

2. Compute the nodal gradients $\nabla\tilde{U}$.

$$(\vec{\nabla}\tilde{U})_i = \frac{1}{meas(C_i)} \sum_{T \in C_i} \frac{meas(T)}{3} \sum_{k \in T} (\tilde{U})_k \vec{\nabla} \Phi_k^T \tag{51}$$

3. Start *edgewise assembly loop*:
compute the extrapolated slopes :

$$\begin{aligned} (\vec{\nabla}\tilde{U})_{ij} \cdot \vec{ij} = \quad & (1-\beta)(\vec{\nabla}\tilde{U}))^c_{ij} \cdot \vec{ij} + \beta(\vec{\nabla}\tilde{U}))^u_{ij} \cdot \vec{ij} \\ & +\xi_c \left[(\vec{\nabla}\tilde{U}))^u_{ij} \cdot \vec{ij} - 2(\vec{\nabla}\tilde{U}))^c_{ij} \cdot \vec{ij} + (\vec{\nabla}\tilde{U}))^d_{ij} \cdot \vec{ij} \right] \\ & +\xi_d \left[(\vec{\nabla}\tilde{U}))_{D^*_{ij}} \cdot \vec{ij} - 2(\vec{\nabla}\tilde{U}))_i \cdot \vec{ij} + (\vec{\nabla}\tilde{U}))_j \cdot \vec{ij} \right] \quad , \end{aligned} \tag{52}$$

and analog for $\vec{\nabla}(\tilde{U})_{ji}$.
Define left and right variable interpolations:

$$\begin{aligned} \tilde{U}_{ij} &= \tilde{U}_i + \nabla\tilde{U}_{ij} \\ \tilde{U}_{ji} &= \tilde{U}_j - \nabla\tilde{U}_{ji} \end{aligned} \tag{53}$$

And recover the left and right values of conservative variables U_{ij}, U_{ji}. The upwind differenced flux then writes:

$$\Phi_{ij} = \Phi^{Riemann}(U_{ij}, U_{ji}) \tag{54}$$

and add (substract) it to flux assembly at vertex i (j) and multiply flux assembly by the inverse mass matrix in order to obtain the update of the variable.

We recall that for $\beta = \xi_c = \xi_d = 0$, this scheme is fourth-order accurate, see [15], but the scheme may lack dissipation for our purpose. Each term in ξ_c or ξ_d introduces a fifth-order derivative (multiplied by flux's Jacobian F') in the modified equation, except in the case where $\xi_c = -\xi_d$, which produces a sixth-order dissipation with $O(\Delta x^5)$ weigth in Cartesian

$\Delta x = \Delta y$ case. In order to be at same level of dissipation as for **FE-NLV6**, we suggest to take:

$$\xi_c = -\frac{3\delta}{30} \ , \quad \xi_d = \frac{3\delta}{30} \ .$$

Remark: In order to recover consistency for stretched meshes, a modification similar to the one applied to **FE-NLV6** is necessary.

4.4 Boundary conditions

Boundary conditions have a crucial influence on the quality of practical acoustic simulations. Non-reflecting boundary conditions are necessary in order to avoid spurious reflecting waves to travel in the computational domain. In this preliminary study, we shall not consider problems with possible reflections, and we shall use in the presented calculations upwind farfield conditions relying on the Steger-Warming flux splitting. In short, fluxes between boundary cell and external medium are computed as follows:

$$\Phi_i^{external} \ = \ A^+(U_i)U_i \ + \ A^-(U_\infty)U_\infty$$

where $A = \frac{\partial F}{\partial U} \cdot n$, n being the normal to boundary, U_∞ the background flow and perturbation specified at farfield.

4.5 Time advancing

As explicit time advancing we can use, as in the 1D case, a standart Runge-Kutta scheme or the linearized version defined above. We observe that for FV versions, time-steps are comparable to usual upwind schemes, and for FE versions, time-steps are three times smaller. An implicit Backward-Differencing formula can also be applied with a spatially-first-order accurate simplified Jacobian. An interesting option is a second-order Backward-Differencing formula applied also with a spatially-first-order accurate simplified Jacobian under the form of a two-step-Newton Defect Correction as in [20].

5 In three dimensions

5.1 Upwind elements

As in 2D, the element T_{ij} is *upwind* to the vertex i with respect to the edge ij if, for any small enough real number η, the vector $-\eta\vec{ij}$ is inside the element T_{ij}. Symmetrically, the element T_{ji} is *downwind* to the vertex i with respect to the edge ij if, for any small enough real number η, the vector $\eta\vec{ji}$ is inside h real element T_{ij}. This is sketched in Figure 7.

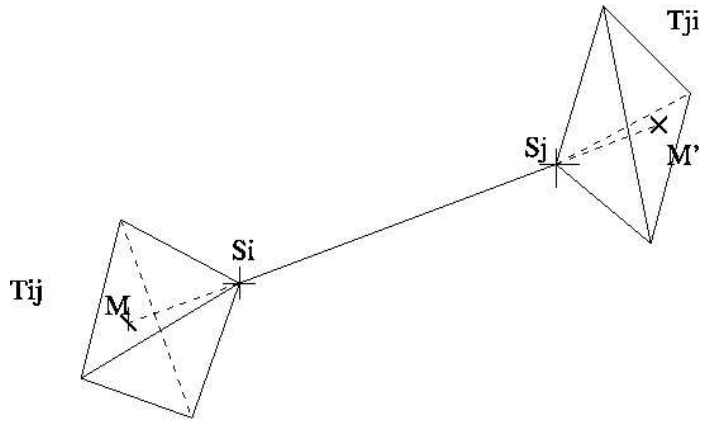

Figure 7: Edge-upwind tetrahedra

5.2 Medians cells

Extension to 3-D of median cells is not complicated. OnThey are made by the common surface between two vertices of an element and the triangles connecting:

- the middle of the bar linking the considered apices,
- the center of gravity of the faces of the element having this bar as an edge,
- the center of gravity of the element.

By analogy with 2-D, one should rather construct cells as regular as possible when the mesh is non-structured. Then, one would wish the cells be rectangle parallelepipeds centered around the apices when the mesh is the 3-D equivalent to Friedrichs-Keller mesh. First, it is important to define the shape of the volumetric elements.

5.3 Superconvergent tetrahedrization

N. Gourvitch proposed to use the combination of a particular splitting of cubes into tetrahedra and of splitting of a tetrahedron into part of cells centered around each vertex, see for example [21]. We recall these techniques in the next two sections.

In 3-D, space is first divided into hexahedra. For sake of simplicity, the case of a Cartesian mesh is considered. Thus, we consider rectangles parallelepipeds (thereafter called *blocks*), whose volumes are $V_0 = \Delta x \times \Delta y \times \Delta z$. It is desirable to end up with tetrahedral elements; thus, one must divide these blocks. In Table 11, we define three different ways to do this. The two first ones are standard. The first division (**D1**) minimizes the number of sub-tetrahedra, but generates a big central element, (volume $=V_0/3$), and four peripheral elements (Volume

$= V_0/6$). The second division (**D2**) yields two identical prisms, each being subdivided into three tetrahedra. These tetrahedra are not similar, some of them involve a vertex with three angles of $\pi/2$, while and the central ones do not and have rather small and large angles. For both (**D1**) and (**D2**) divisions, the resulting dual cells are rather unsymmetrical. In order to get dual cells that are as regular as possible, and to come back to a Finite Differences scheme, a 3-D adapted division is built The (**"New Generation"** Division, or **NGD**) splits the *block* in six identical tetrahedra, with volumes $V_0/6$, each being the image of its neighbors in a mirror. All these elements have in common a diagonal of the *block*. The coordinates of the tetrahedra resulting from the three divisions are shown in Figures 10 and 11, depending upon the local numbers of the block vertices. Figures 8 and 9 show the **D1** and **NGD** divisions.

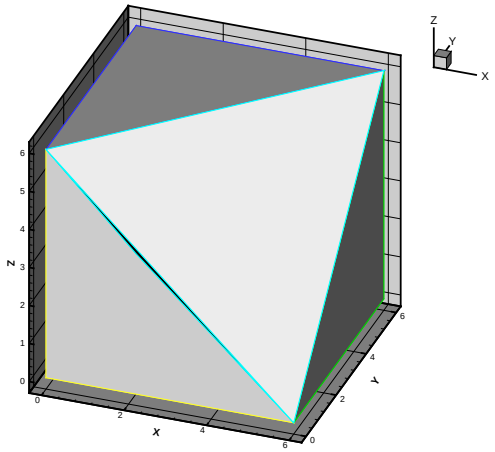

Figure 8: **D1** division

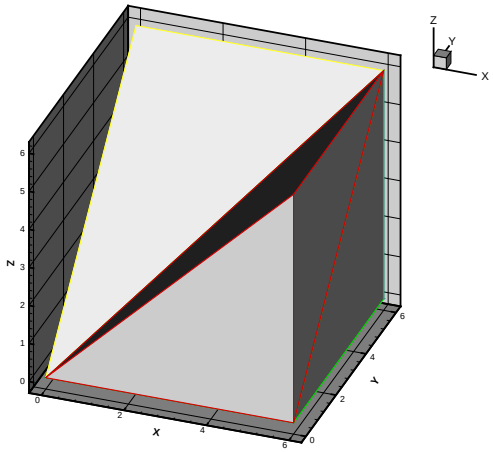

Figure 9: **NGD** division

Lemma 1: *In the case of a conformal tetrahedrization obtained by dividing a regular grid of parallelepiped with fixed* $\Delta x, \Delta y, \Delta z$*, an element-wise* x*-derivative (resp.* y*-derivative,* z*-derivative) is computed from only two vertices, aligned with the* x*-direction (resp.* y*-direction,* z*-direction); a nodal* x*-derivative (resp.* y*-derivative,* z*-derivative)is computed from exactly three vertices, aligned with the* x*-direction (resp.* y*-direction,* z*-direction).*□

5.4 NGC cells [21]

"New Generation Cells" (or **NGC**) denotes the group of polyhedra such that, for a given element, the common surface between two neighboring vertices joins:

- the middle of the edge connecting these two vertices,

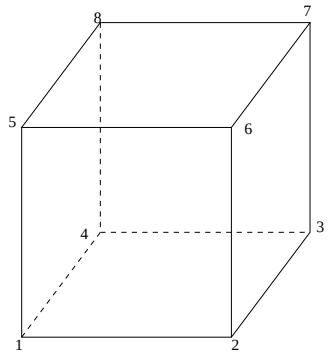

Figure 10: Local numbering of vertices in a *block*

Element	vertices		
	D1	**D2**	**NGD**
1	(2,6,7,5)	(1,2,3,6)	(2,1,4,6)
2	(2,3,4,7)	(1,5,6,7)	(3,2,4,6)
3	(5,8,7,4)	(6,1,7,3)	(7,3,4,6)
4	(1,2,4,5)	(1,5,7,8)	(8,7,4,6)
5	(2,5,7,4)	(1,7,3,8)	(5,8,4,6)
6		(1,3,4,8)	(1,5,4,6)

Figure 11: Sub-tetrahedra vertices identified from local block numbering for the three different splitings

- the **"surface center"** of the faces of the element having this edge in common,
- the "volume center" of the element,

where

- the **"surface center"** of a given face is its c.c.c. if it comprises only acute angles otherwise, it is the closest point of the triangle, i.e. the middle of its longest edge,
- the **"volume center"** of an element is its c.c.s. if the former is located inside the element; otherwise, it is the closest point, i.e. the **"surface center"** of the largest surface.

One can notice that when tetrahedra result from **NGD** then all the elements faces are rectangle triangles. In this case, the cell joins the middle of the longest edge of the tetrahedron to the middles of the other edges. The cells generated in this way are blocks, centered around the vertices of the mesh. Figures 12 and 13 show the trace of the division of an element into cells, according to the old and new methods, respectively.

Lemma 2: *In the case of a conformal tetrahedrization obtained by dividing a regular grid of parallelepiped with fixed* $\Delta x, \Delta y, \Delta z$*, the new* **FE-NLV6** *scheme finite-volume formulation reduces to the usual one with cubes.* □

Lemma 3: *In the case of a conformal tetrahedrization obtained by dividing a regular grid of parallelepiped with fixed* $\Delta x, \Delta y, \Delta z$*, the new* **FE-NLV6** *scheme is fifth-order accurate in space.* □

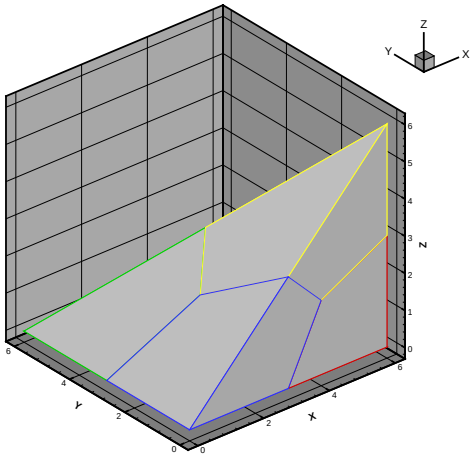

Figure 12: Trace of medians cells on a tetrahedron resulting from **NGD**

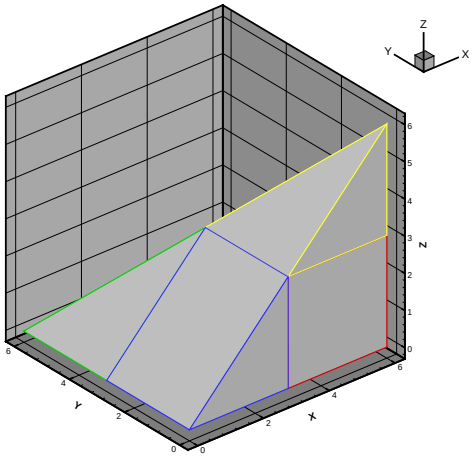

Figure 13: Trace of **NGC** on a tetrahedron resulting from **NGD**

6 Conclusion

We have proposed a new family of schemes for the Euler equations. This family extends the V6 family studied in [15][16][17] [1] [2][3][4][5] [9][10][11] [21].
The **LV6** schemes of [15][16][17] [9][10][11] were based on MUSCL schemes, involving sophisticated primitive variable reconstruction in order to enjoy low dissipation properties, due to the related dissipation, which is based on a model of sixth derivative. In the case of advection with uniform velocity, those schemes present superconvergence properties, in the sense that, when applied to a Cartesian subregion of mesh, these second-order schemes are of higher order (up to sixth-order) .

The main novelty of the present work concerns the reconstruction of flux functions instead of primitive variables. Upwinding is made through sign-based Riemann solvers for using only flux values. The proposed schemes still apply to unstructured triangulations with second-order accuracy where they stay essentially second-order accurate, and involve a tunable small stabilisation term made with a sixth-order derivative. The accuracy is much better that for usual second-order schemes.
In contrast to **LV6** schemes, the new **NLV6**schemes enjoy superconvergence properties also for *nonlinear arbitrary fluxes*. Superconvergence order of accuracy is between 4 and 6.

FV-V6NL: the first family of schemes is of MUSCL type. The schemes can be explicit without any matrix inversion (lumped/diagonal or finite-volume mass matrix). Stability condition for multistage time advancing allows Courant number more that unity.
For a bounded stretching, up to six-order accuracy is reached for Cartesian meshes with the median cell construction, but consistency is lost for arbitrary stretching.

Sixth-order accuracy is reached for Cartesian meshes without limitation on stretching when the following options are applied :
- the Barth cell construction,
- Gourvitch splitting of cubes.
On non-Cartesian mesh, accuracy lies between first-order and second-order, depending on the mesh regularity. Explicit time advancing does not require mass matrix solution.

FE-V6NL: the second family uses the finite-element consistent mass matrix. Only median cells can be considered for accuracy. Explicit time advancing requires mass matrix solution. Stable time steps are typically three times smaller than with the first FV-V6NL family. Then explicit time stepping can be more expensive. On Cartesian meshes, accuracy can be of fourth-order at least in 2D case. On non-Cartesian mesh, accuracy remains second-order on arbitrary meshes, in particular, we expect that accuracy will be better for meshes in which mesh size varies rather suddenly. Stretched meshes should also be well accepted by this approximation. Spatial accuracy is conserved in the case of implicit time advancing, and in this case the mass matrix does not carry extra cpu cost.

These schemes have been introduced into a LES CFD software and numerical experiments for **FV-V6NL** and **FE-V6NL** will be shown in a report following this one.

References

[1] I. Abalakin, A. Dervieux, and T. Kozubskaya. A vertex centered high-order MUSCL scheme applying to linearised Euler acoustics. *Research report INRIA, No. 4459*, 2002.

[2] I. Abalakin, A. Dervieux, T. Kozubskaya. Computational Study of Mathematical Models for Noise DNS, *AIAA paper* 2002-2585

[3] I. Abalakin, A. Dervieux, T. Kozubskaya. High Accuracy Study of Mathematical Models for DNS of Noise around Steady Mean Flow, in Proc. of *West East High Speed Flow Field Conference 2002*, D.E. Zeitoun, J. Periaux, J.A. Desideri, M. Marini (Eds.), CIMNE, Barcelona (2002)

[4] I. Abalakin, V. Bobkov, A. Dervieux, T. Kozubskaya, V. Shiryaev, Study of high accuracy order schemes and non-reflecting boundary conditions for noise propagation problems, Liapunov Institute report, project 99-02, 2001, available on : http://www-sop.inria.fr/tropics/Alain.Dervieux/liapunov.html

[5] I. Abalakin, A. Dervieux, T. Kozubskaya. On accuracy of noise direct calculation based on Euler model, *Int. J. Acoustics* Vol. 3, N 2, 2004, pp. 157-180

[6] R. Abgrall. An essentially non-oscillatory reconstruction procedure on finite element type meshes, application to compressible flows. *Computer Methods in Applied Mechanics and Engineering*, **116**, 1994, 95-101.

[7] T. Barth. Aspects of Unstructured Grids and Finite-Volume Solvers for the Euler and Navier-Stokes Equations, in *Special Course on Unstructured Grid Methods for Advection Dominated Flows, AGARD report 787*, p. 6-1 to 6-61, 1992.

[8] F. Bassi, S. Rebay. A high-order accurate discontinuous finite element method for the numerical solution of the compressible Navier-Stokes equations. *Journal of Computational Physics*, **131**, 1997, 267-279.

[9] S. Camarri, M.V. Salvetti, B. Koobus, A. Dervieux. Numerical diffusion based on high-order derivatives in MUSCL schemes for LES on unstructured grids, in the proceedings of *DLES-4, Direct and Large-Eddy Simulation-IV*, July 18-20,2001, Twente (Holland)

[10] S. Camarri, M.-V. Salvetti, A. Dervieux, B. Koobus. A low diffusion MUSCL scheme for LES on unstructured grids, *Research report INRIA, No. 4412*, July 2002

[11] S. Camarri, B. Koobus, M.V. Salvetti andA. Dervieux. A low-diffusion MUSCL scheme for LES on unstructured grids. *Computers and Fluids*, Vol.33. 1101-1129, 2004

[12] R. Carpentier. *Approximation d'écoulements instationnaires. Application à des instabilités tourbillonnaires.* Thesis, University of Nice-Sophia Antipolis, 1995.

[13] R. Carpentier. Schéma de haute précision en maillage quadrangulaire structuré pour des écoulements compressibles non visqueux (in french), *Research report INRIA, No.3909* , april 2000

[14] P.-H. Cournède, B. Koobus and A. Dervieux. "Positivity statements for a Mixed-Element-Volume scheme on fixed and moving grids. *Revue Européenne de Mécanique Numérique*, 15:7-8, 767-799, 2006

[15] C. Debiez Approximation et linearisation d'ecoulements aerodynamiques instattionnaires. Thesis, University of Nice-Sophia Antipolis, 1996.

[16] C. Debiez, A. Dervieux. Mixed Element Volume MUSCL methods with weak viscosity for steady and unsteady flow calculation. *Computers and Fluids*, 1999,**29**, 89-118

[17] C. Debiez, A. Dervieux, K. Mer, and B. NKonga. Computation of unsteady flows with mixed finite/finite element upwind methods. *International Journal for Numerical Methods in Fluids*, 1998, **27**, 193-206.

[18] A. Dervieux. Steady Euler Simulations Using Unstructured Meshes. Von Karman Institute for Fluid Dynamics, Lecture series 1985-04, Computational Fluid Dynamics (1985). Revised version published as a chapter of "Partial Differential Equations of hyperbolique type and Applications", Geymonat Ed., World Scientific, Singapore, 1987.

[19] J-A. Desideri, A. Goudjo, and V. Selmin. Third-order numerical schemes for hyperbolic problems. *Research report INRIA, No. 607*, 1987.

[20] R. Martin and H. Guillard A second-order defect correction scheme for unsteady problems *Computer and Fluids* **25**:9-27, 1996

[21] N. Gourvitch, G. Rogé, I. Abalakin, A. Dervieux, T. Kozubskaya, A tetrahedral-based superconvergent scheme for aeroacoustics, *Research report INRIA, No. 5212*, May 2004

[22] "ICASE/LaRC Workshop on Benchmark Problems in Computational Aeroacoustics(CAA)", NASA Conference Publication, Hampton, Virginia, October 24-26, 1994.

[23] A. Jameson. Artificial diffusion, upwind biasing, limiters and their effect on accuracy and multigrid convergence in transonic and hypersonic flows. *AIAA paper 93-3359.* AIAA 11th Computational Fluid Dynamics Conference, Orlando, FL,1993.

[24] B. van Leer. Towards the Ultimate Conservative Difference Scheme I. The Quest of Monotonicity, *Lectures notes in Physics*, 1972, **18**, p.163

[25] S. Lemaire, G. Rogé. Aéroacoustique appliquée aux avions d'affaires: Problématique, méthodologie et outils envisagés chez Dassault Aviation (in french) *38ème colloque d'aérodynamique appliquée Aéroacoustique des véhicules aéronautiques et terrestres, AAAF*, Arcachon 7-9 octobre 2002,

[26] C. K. W. Tam, J. C. Webb, Dispersion-Relation-Preserving Finite Difference Schemes for Computational Acoustics. *Journal of Computational Physics*, **107**, 261-281, 1993.

[27] C. Viozat, C. Held, K. Mer, A. Dervieux, On Vertex-centered unstructured finite-volume methods for stretched anisotropic triangulations. *Computer Meth. in Applied Mech. and Eng.*, 190 (35-36), pp.4733-4766, 2001.

[28] H. Wu, L. Wang. Non-existence of third-order accurate semi-discrete MUSCL-type schemes for nonlinear conservation laws and unified construction of high accurate ENO schemes. *Sixth International Symposium on Computational Fluid Dynamics*, September 4-8, 1995, Lake Tahoe, NV.

Unité de recherche INRIA Sophia Antipolis
2004, route des Lucioles - BP 93 - 06902 Sophia Antipolis Cedex (France)

Unité de recherche INRIA Futurs : Parc Club Orsay Université - ZAC des Vignes
4, rue Jacques Monod - 91893 ORSAY Cedex (France)
Unité de recherche INRIA Lorraine : LORIA, Technopôle de Nancy-Brabois - Campus scientifique
615, rue du Jardin Botanique - BP 101 - 54602 Villers-lès-Nancy Cedex (France)
Unité de recherche INRIA Rennes : IRISA, Campus universitaire de Beaulieu - 35042 Rennes Cedex (France)
Unité de recherche INRIA Rhône-Alpes : 655, avenue de l'Europe - 38334 Montbonnot Saint-Ismier (France)
Unité de recherche INRIA Rocquencourt : Domaine de Voluceau - Rocquencourt - BP 105 - 78153 Le Chesnay Cedex (France)

Éditeur
INRIA - Domaine de Voluceau - Rocquencourt, BP 105 - 78153 Le Chesnay Cedex (France)
http://www.inria.fr
ISSN 0249-6399